PNAS
www.pnas.org

Supplementary Information for

POLArIS, a versatile probe for molecular orientation, revealed actin filaments associated with microtubule asters in early embryos

Ayana Sugizaki, Keisuke Sato, Kazuyoshi Chiba, Kenta Saito, Masahiko Kawagishi, Yuri Tomabechi, Shalin B. Mehta, Hirokazu Ishii, Naoki Sakai, Mikako Shirouzu, Tomomi Tani, Sumio Terada*

* Sumio Terada
Email: terada.nana@tmd.ac.jp

This PDF file includes:

SI Materials and Methods
Figures S1 to S9
Tables S1
Legends for Movies S1 to S11
SI References

Other supplementary materials for this manuscript include the following:

Movies S1 to S11

SI Materials and Methods

Cell culture

HeLa cells (a generous gift from Dr. Yoshimori, Osaka University) and HeLa M cells (a generous gift from Dr. Lowe, University of Manchester) were incubated at 37°C in Dulbecco's modified Eagle medium (DMEM, nacalai tesque) containing 10% fetal bovine serum (FBS) with 5% CO_2. LLC-PK1 cells (EC86121112-F0, ECACC) were incubated at 37°C in Medium 199 (Merck) containing 10% fetal bovine serum (FBS) with 5% CO_2. XTC cells (a generous gift from Dr. Mitchell, Northwestern University) were incubated at room temperature in 70% Leibovitz's L-15 medium (Thermo Fisher Scientific) containing 10% FBS.

Plasmid construction

Sequence information of binding domains of Adhirons used in this study was described at the 60th Annual Meeting of Biophysics Society (1). DNA fragments of Ad-A, B, and C were synthesized by GeneArt Strings DNA Fragments (Thermo Fisher Scientific). The sequences for a fusion protein consisting of circularly permutated GFP (cpGFP; developed in our lab (2)) and each Adhiron were amplified by PCR using PrimeSTAR MAX (TAKARA Bio) and inserted in modified pcDNA3 vector (3), so that these two proteins are connected by a flexible linker. Then the flexible linker was replaced with 11 different linker sequences shown in Fig. S1A using typical restriction enzyme cloning methods.

To make plasmids for mRNA synthesis, the POLArIS^{act} sequence and EMTB-mCherry (Addgene plasmid 26742) sequence were amplified by PCR and subcloned into the pGEMHE vector using Gibson Assembly.

Protein purification and electrophoresis

The coding sequence for cpGFP, Ad-A, or POLArIS^{act} was inserted into the C-terminus of His tag in the pRSET B bacterial expression vector. *E. coli* JM109 (DE3) transformed with these plasmids were precultured in LB medium for 6 h at 37°C, diluted in LB medium at 1:1000, and cultured again for 72 h at 20°C. Cells of *E. coli* were collected by centrifugation and resuspended in TN buffer (50 mM Tris-HCl, 300 mM NaCl, pH 7.4). After cell disruption by sonication, the protein was purified using affinity purification with Ni Sepharose 6 Fast Flow (Cytiva). Samples were subjected to SDS-PAGE and the gels were stained with CBB staining using Quick-CBB PLUS (FUJIFILM Wako Pure Chemical).

Crystallization and structure determination

Sequence coding POLArIS^{act} T57S mutant was cloned into pET24a bacterial expression vector, so that the N-terminal T7 peptide sequence was removed and the TEV cleavage site was inserted between the C-terminus of Adhiron and the N-terminus of His tag. The generated plasmid was transformed into *E.coli* Rosetta (DE3) and the protein was over-

expressed overnight at 20°C in LB medium with induction by 0.3 mM IPTG. The cells were collected and were lysed using a sonicator. After centrifugation, the supernatant was applied on a HisTrap HP column (Cytiva) and the target protein was eluted with a linear gradient of imidazole. The His tag was then cleaved by TEV protease and was removed by a HisTrap HP column. The protein was further purified by ion-exchange on a HiTrap Q column (Cytiva) and by size-exclusion chromatography on a HiLoad 16/60 Superdex 75 pg column (Cytiva) in a buffer containing 25 mM Hepes-NaOH (pH 7.5), and 150 mM NaCl.

Crystals were grown at 20°C by the method of sitting drop vapor diffusion with a reservoir solution containing 0.1 M sodium acetate (pH 4.5-5.0) and 6-8% (v/v) PEG 4000. Crystals were cryo-protected with the reservoir solution containing 25% glycerol. Diffraction data were collected at a wavelength of 1.0 Å at SLS beamline X06DA (Villigen). Data were processed with the XDS programs (4) and the structure was solved by molecular replacement using the Phaser program (5) from the PHENIX programs (6), with the superfolder GFP (PDB ID:4LQT) and the Adhiron (PDB ID:4N6U) as the search models. The structural model was built into the electron density map using COOT (7) and refined using the PHENIX program and Refmac5 from the CCP4 program suite (8). The final statistics are summarized in Table S1.

Structural modeling of cpGFP-Adhiron fusion

Modeling of the fusion of proteins was performed on UCSF Chimera (9). The structure of cpGFP was made by modifying the structure of the superfolder GFP (PDB ID:4LQT) and fused with Adhiron (PDB ID:4N6U) with manually constructed linker structures.

Pull-down assay

G- and F-actin were prepared from rabbit skeletal muscle actin (AKL99, Cytoskeleton) following the manufacturer's protocol. To depolymerize actin oligomers, actin protein was suspended to 0.4 mg/ml in general actin buffer (5 mM Tris-HCl, 0.2 mM $CaCl_2$, 0.2 mM ATP, 0.5 mM DTT, pH 8.0) and incubated for 1 h on ice. After centrifugation at 4°C for 1 h, at 55,000 rpm using a fixed angle rotor S120AT2 (himac), the supernatant was used as a G-actin solution. To prepare F-actin solution, G-actin suspended in polymerization buffer (5 mM Tris-HCl, 50 mM KCl, 2 mM $MgCl_2$, 0.2 mM $CaCl_2$, 1.2 mM ATP, 0.5 mM DTT, pH 8.0) was incubated at room temperature for 1 h.

Proteins were mixed at the concentrations indicated in Fig. S4B in 200 µl of general actin buffer (for samples containing G-actin) or polymerization buffer (for samples containing F-actin). After incubation at room temperature for 1 h, 20 µl was taken from each sample as an "input" fraction, and the remaining 180 µl was added to 10 µl of washed beads of Ni Sepharose 6 Fast Flow and incubated at room temperature for 1 h with gently mixing. After centrifugation, the supernatant was collected as an "unbound" fraction. Precipitated beads were washed with general actin buffer (G-actin samples) or polymerization buffer (F-actin samples), followed by centrifugation again, and the

supernatant was removed. The beads remained were used as “bound” fraction. Each fraction was mixed with SDS sample buffer, incubated at room temperature for 1 h, and then boiled at 95°C for 10 min. These samples were subjected to SDS-PAGE with 8% or 5-11% Bullet PAGE One Precast Gel (nacalai tesque) and the gels were stained using Quick-CBB PLUS.

Scanned images of gels from three independent sets of assays were quantified using ImageJ. *P* values were manually calculated on Microsoft Excel by applying Šidák multiple comparison correction to Student’s t-test, and difference with $p < 0.01$ was considered significant.

Co-sedimentation assay

F-actin was prepared in the same way as in pull-down assays. F-actin and POLArIS^{act} were mixed in 50 µl of polymerization buffer with a concentration of 2.5 µM and 1-10 µM, respectively. After incubation at room temperature for 30 min, the mixture was centrifuged at 4°C for 1 h, at 55,000 rpm. The supernatant and the pellet were mixed with SDS sample buffer and were boiled at 95°C for 10 min. Ad-A and sfGFP instead of POLArIS^{act} were assayed in the same way as controls. These samples were analyzed by SDS-PAGE using home-made 8% or 12% acrylamide gel and the gels were stained using Quick-CBB PLUS.

Scanned images of gels from three independent sets of assays were quantified using ImageJ. Based on experimental assumptions that POLArIS^{act} binds to F-actin with 1:1 stoichiometry, which is determined from the result that approximately up to 2.5 μM POLArIS^{act} was co-sedimented with 2.5 μM F-actin, the dissociation constant (K_d) was obtained according to the definition. Each actual value when the concentration of POLArIS^{act} was 1.5-2.5 μM in three sets of assays was substituted into the equation of definition to obtain K_d,, and the average of values from three experiments was calculated.

Plasmid introduction into cultured cells

cpGFP-Adhiron expression plasmids were transfected into HeLa or XTC cells cultured on glass-bottom dishes or coverslips using Lipofectamine LTX or 3000 (Thermo Fisher Scientific). The medium was replaced with fresh medium approximately 5 h after transfection. For HeLa M transfection, Polyethylenimine "Max" (24765-1, Polysciences) was used for transfection. For LLC-PK1, the NEPA21 electroporator (Nepagene) was used to introduce plasmids into cells. For live-cell imaging, the medium was replaced with DMEM/Ham's F-12 without phenol red (nacalai tesque) or Medium 199 without phenol red (Thermo Fisher Scientific) containing 10% FBS before observation.

Fixation and staining of cultured cells

To examine the co-localization of cpGFP-Adhiron and F-actin using fluorescently labeled phalloidin, transfected cells were washed with phosphate-buffered saline (PBS), and then fixed with 4% paraformaldehyde in PBS (pH 7.4). After permeabilization with 0.1% TritonX-100 for 5 min, the specimens were incubated with 0.5 μg/ml of phalloidin-Atto565 (94072, Merck), 2 μg/ml of Hoechst 33342 (04915-81, nacalai tesque), and 5% skimmed milk in PBS for 1 h at room temperature. Stained cells were washed with PBS and mounted in a mounting solution made of Mowiol 4-88 (ITW Reagents).

In vitro preparation of F-actin and labeling

Purified human platelet actin (APHL99, Cytoskeleton) was polymerized following the manufacturer's protocol and attached to polylysine coated coverslips by incubation with 2 μg/ml actin in actin polymerization solution. Then, specimens were incubated with 10 nM purified recombinant POLArIS^{act} protein or 2-5 nM Alexa Fluor 488 Phalloidin (AF488-phalloidin, A12379, Thermo Fisher Scientific) and 10 mg/ml bovine serum albumin (BSA) in actin polymerization solution for 5 min.

Starfish egg preparation and drug treatment

Asterina pectinifera starfishes were collected on the Pacific coast of Japan and were kept in laboratory aquaria with seawater at 14–15°C. Immature oocytes of *Asterina pectinifera* starfishes were treated with cold calcium-free seawater to remove follicle

cells, and then incubated in filtered seawater. Oocytes were microinjected with the mRNA encoding POLArIS^{act}, UG3, and/or EMTB-mCherry (synthesized *in vitro* from linearized DNA templates using the mMessage mMachine T7 ULTRA Transcription kit (Thermo Fisher Scientific)) on the day before observation and incubated in filtered or artificial seawater (ASW: 423 mM NaCl, 9 mM KCl, 23 mM $MgCl_2$, 25 mM $MgSO_4$, 9 mM $CaCl_2$, 10 mM HEPES, pH 7.4) at 16°C overnight. After POLArIS^{act} and/or EMTB-mCherry were expressed at the appropriate level, oocytes were treated with 1-Methyladenine (1-MA, KANTO CHEMICAL) to induce maturation.

For observation of early development processes, oocytes were inseminated after germinal vesicle breakdown (GVBD) and incubated at 16°C until microscopic imaging was started. In pharmacological experiments, embryos were treated with 20 µM nocodazole (NCZ) (487929, Merck), 10 µM cytochalasin D (CytoD) (C8273, Merck), 200 µM CK666 (182515, Merck) or 10 µM SMIFH2 (344092, Merck) in ASW at the indicated timing (see figure legends for details), or perfused with 10 µM SMIFH2 dissolved in ASW by inserting a microneedle into the perivitelline space after fertilization envelope formation. In control experiments, embryos were exposed with ASW containing DMSO. Drugs were diluted in ASW from stock solutions dissolved in DMSO (NCZ, 10 mM; CytoD, 10 mM; CK666, 100 mM; SMIFH2, 50 mM) and the same volume of DMSO as the volume of each stock solution was added to ASW as control.

For observation of fertilization, 1-MA treated eggs were inseminated after GVBD. To perform simultaneous observation of F-actin and DNA, immature eggs were pre-stained

with 10 µg/ml Hoechst 33342 for 30 min. Stained eggs were washed with ASW and then treated with 1-MA. Sperms were also stained with 10 µg/ml Hoechst 33342 for 5 min just before insemination.

Fixation and fluorescent phalloidin staining of starfish embryos with PFA or PFA+GA

As soon as the green/magenta cross pattern clearly appeared, starfish embryos expressing POLArIS^{act} were fixed for 1 h with 4% PFA in MES buffer (10 mM MES, 150 mM NaCl, 5 mM EGTA, 5 mM glucose, 5 mM $MgCl_2$, pH 6.1) or 0.25% GA and 4% PFA in HEPES buffer (10 mM HEPES, 460 mM NaCl, 10 mM KCl, 36 mM $MgCl_2$, 17 mM $MgSO_4$, pH 8.2) under the FPM. For AF488-phalloidin staining, embryos fixed with GA+PFA in HEPES buffer were then washed with HEPES buffer, and PFA and GA were quenched with 100 mM glycine. After permeabilization for 15 min with HEPES buffer containing 0.1% TritonX-100, embryos were stained for 2 h with AF488-phalloidin.

Immunofluorescence of fixed starfish embryos

Starfish embryos were fixed for 1 h with a 3% v/v glyoxal (17226-95, nacalai tesque) fixative solution prepared as described previously (10). After fixation, embryos were washed with PBSw/NaCl (same as PBS except that NaCl concentration was adjusted at 460 mM) and glyoxal was quenched with 100 mM glycine. Embryos were then permeabilized with PBSw/NaCl containing 0.1% TritonX-100, blocked with 0.05% BSA,

and sequentially incubated with primary and secondary antibodies dissolved in PBSw/NaCl. To visualize microtubules, YL1/2 rat anti-α-tubulin (MCA77G, Bio-Rad) was used as a primary antibody, and goat anti-rat IgG conjugated with Alexa488 (A-11006, Thermo Fisher Scientific) was used as a secondary antibody. To visualize DNA and F-actin, Hoechst 33342 and phalloidin-Atto565 were used, respectively. Stained embryos were placed on a MAS-coated slide glass (Matsunami Glass), mounted with SlowFade Diamond (S36963, Thermo Fisher Scientific), covered with a coverslip, and sealed with nail polish. The observation was carried out within 2 days, as staining with phalloidin-Atto565 was blurred 3 days after glyoxal fixation.

Fluorescence microscopy

Fluorescence microscopic observation of fixed HeLa cells was performed with the Nikon Eclipse E600 microscope with a dry objective lens (PlanFluor 40x 0.75 N.A., Nikon) or an oil immersion objective lens (PlanFluor, 100x 1.30 N.A., Nikon). Images were acquired with the application software ACT-2U (Nikon), and then processed with ImageJ.

Fluorescence microscopic observation of living starfish eggs/embryos and data acquisition were performed with Nikon Eclipse TiE microscope with dry objective lenses (PlanApo 10x 0.45 N.A., and 20x 0.75 N.A., Nikon) and silicone oil immersion objective lenses (UPLSAPO, 30x 1.05 N.A., and 40x 1.25 N.A., Olympus) in a room kept at 20°C.

Fluorescence microscopic observation of fixed starfish eggs/embryos and data acquisition were performed with Nikon C1 CLSM with a silicone oil immersion objective lens (UPLSAPO, 40x 1.25 N.A., Olympus), Leica SP8 CLSM (Leica) with an oil immersion objective lens (HC PL APO 63x/1.40 Oil CS2, Leica), or Carl Zeiss LSM510 CLSM with a water immersion objective lens (C-Apochromat 40x/1.2 W Corr, Carl Zeiss). Images were taken with NIS-Elements Advanced Research, Leica LAS X, and Zeiss ZEN, respectively, and processed with ImageJ.

Two-axis Fluorescence Polarization Microscopy

The polarization beam splitting system was assembled at the detection port of Nikon Eclipse TiE (2). In brief, samples were illuminated by the isotropically polarized LED light from SPECTRA light engine (lumencor) and the linear polarization beam splitter splits fluorescence into two orthogonal polarization orientations, 0° (horizontal orientation) and 90° (vertical orientation), and detected with a single camera (iXon3 897 EM-CCD (Andor Technology) or Zyla 4.2 plus sCMOS (Andor Techonology)). Both polarization images were labeled with pseudo-colors (horizontal polarization, green; vertical polarization, magenta) with NIS-Elements Advanced Research. Images of merged color were shown in real-time with the dual-view function of NIS-Elements Advanced Research. We used dry objective lenses (PlanApo 10x 0.45 N.A., and 20x 0.75 N.A., Nikon) and silicone oil immersion objective lenses (UPLSAPO, 30x 1.05 N.A., and 40x 1.25 N.A., Olympus). iXon3 897 EM-CCD camera (Andor Technology) and Zyla 4.2 plus

sCMOS (Andor Techonology) were used for detection. Filter cube LF488-C (Semrock) was used for cpGFP-Adhiron fluorescence.

Instantaneous FluoPolScope

Imaging and analysis using Instantaneous FluoPolScope were performed as reported previously (2, 11). The excitation illumination achieves isotropic polarization at the specimen plane. Fluorescence images were collected with a high NA objective lens (PlanApo TIRF 100x 1.49NA oil, Nikon). In the collimated space, linear polarization beam splitters separate the fluorescence into four images and analyze their linear polarization along 0°, 45°, 90°, and 135° orientations. Based on the intensity imbalance of polarized fluorescence along four orientations, polarization factor and the orientation of maximum polarization of the objects are computed.

Image analysis for fluorescent microscopy

The intensity profiles of fixed HeLa cells were obtained using ImageJ.

The length of actin bundles (from the point on the cell surface where the bundle appears to the tip of the bundle) in starfish oocytes during fertilization were measured using the Nikon imaging software NIS-Elements Advanced Research. Analyses were performed on 8 different zygotes.

Calculation of the polarization value (PV)

For quantification of fluorescence anisotropy of cpGFP-Adhiron constructs, transfected HeLa M cells were arrested in mitosis using the thymidine-NCZ method. In brief, HeLa M cells were treated with 2 mM thymidine for 20 h, and released for overnight in the presence of 100 ng/mL NCZ. We defined Polarization Value (PV) as

$$\mathrm{PV} = \frac{I(\mathrm{Ver})^{\mathrm{norm}} - I(\mathrm{Hor})^{\mathrm{norm}}}{I(\mathrm{Ver})^{\mathrm{norm}} + I(\mathrm{Hor})^{\mathrm{norm}}} ,$$

where $I(\mathrm{Ver})^{\mathrm{norm}}$ = [cortex ROI intensity (Ver) – background (Ver)], $I(\mathrm{Hor})^{\mathrm{norm}}$ = [cortex ROI intensity (Hor) – background (Hor)]·CF, and CF = total intensity (Ver) / total intensity (Hor). The mean intensity of a small rectangle ROI enclosing vertical cortex in the cross-section of a mitotic cell was measured both in vertical polarization and horizontal polarization images to calculate cortex ROI intensity (Ver) and cortex ROI intensity (Hor), respectively. The mean intensity of a square ROI outside of the cell was measured both in the same vertical polarization and horizontal polarization images to calculate background (Ver) and background (Hor), respectively. CF (correction factor) was obtained by calculating the ratio of the mean ROI intensities between vertical and horizontal polarization images that contain a whole cell, using images of cells expressing cpGFP-Ad-A flex. Examples of ROI settings are shown in Fig. S2A. Positive PV values indicate the polarization is parallel to the axis of actin filaments, and negative PV values indicate the perpendicular polarization. n = 10 for each calculation. *P* values against

cpGFP-Ad-A (flex) were manually calculated on Microsoft Excel by applying Šidák multiple comparison correction to Student's t-test. Difference with $p < 0.01$ was considered significant.

Analysis of the cross pattern of FLARE

The presence of the green (horizontal)/magenta (vertical) cross patterns and their centers were deduced using the strategy as detailed below. Suppose a polar coordinate system (r, ϕ) is set over the radial F-actin array, and the transition dipole moments (TDMs) of the fluorophores of POLArIS^{act} are aligned on each F-actin filament. When the fluorophores are excited by vertical polarization (parallel to line ϕ = 0), the fluorescence efficiency of each fluorophore varies with the angle between the polarized excitation and the TDMs. Thus, the distribution of observed fluorescence intensity $Fl_{vertical}$ can be modeled as:

$$\mathrm{Fl}_{\text{vertical}}(r,\varphi) = f_{\text{FLARE}}(r)cos^2(\varphi) + f_{\text{non-radial}}(r,\varphi) + \text{noise},$$

where $f_{\text{FLARE}}(r)$ is the radial profile of the fluorescent component that is aligned on radial F-actin array, and $f_{\text{non-radial}}(r,\varphi)$ is the fluorescent component that is not radially aligned. The distribution of fluorescence intensity $Fl_{horizontal}$ to be observed with horizontal excitation will be:

$$\mathrm{Fl}_{\text{horizontal}}(r,\varphi) = f_{\text{FLARE}}(r)cos^2\left(\varphi - \frac{\pi}{2}\right) + f_{\text{non-radial}}(r,\varphi) + \text{noise}$$

$$= f_{\text{FLARE}}(r)sin^2(\varphi) + f_{\text{non-radial}}(r,\varphi) + \text{noise.}$$

Then the polarization differential image intensity Fl_{diff} of these two will be modeled as:

$$\text{Fl}_{\text{diff}}(r,\varphi) = \text{Fl}_{\text{vertical}}(r,\varphi) - \text{Fl}_{\text{horizontal}}(r,\varphi)$$

$$= f_{\text{FLARE}}(r)cos(2\varphi) + \text{noise.}$$

Thus, fluorophores aligned on a radial F-actin array show a fluorescence intensity pattern that varies with cos(2ϕ) when measured along the circle of fixed radius around the center of the array in the differential image. Conversely, if this characteristic pattern is found on the polarization differential image, it suggests the possible presence of a radial F-actin array there.

Based on this, we used the following algorithm to search for the presence of cross patterns. First, we created a kernel image with this characteristic intensity pattern of cos(2ϕ):

$$\text{pixel value at} \quad (x,y) = (x_{\text{center}} - rsin\varphi, y_{\text{center}} - rcos\varphi) \quad \text{is}$$

$$\begin{cases} \dfrac{cos(2\varphi)}{r_{\text{max}} - r_{\text{min}} + 1} & \text{if} \quad r_{\text{min}} - \dfrac{1}{2} \le r < r_{\text{max}} + \dfrac{1}{2} \\ 0 & \text{otherwise,} \end{cases} ,$$

where $(x_{\text{center}}, y_{\text{center}})$ is the center of the kernel image, and r_{min} or r_{max} specifies the size of the concentric area to look for. Then, we convolved the polarization differential images with this cos(2ϕ) kernel image. Each pixel value of the convolved result is related to the likelihood of the presence of the cos(2ϕ) pattern with the center at that pixel. We

inspected several points with local maximal values as candidates and determined the center of radial F-actin arrays.

The radial extent of the F-actin array was not readily discernable because it was blurred in the noisy background. So, to help visualize the radial profile, we rotated the polarization differential image around the center of the array and calculated the autocorrelation at each radius G_{rot}:

$$G_{\text{rot}}(r,\theta) = \frac{\int_0^{2\pi} \text{Fl}_{\text{diff}}(r,\varphi)\text{Fl}_{\text{diff}}(r,\varphi+\theta)d\varphi}{\int_0^{2\pi}[\text{Fl}_{\text{diff}}(r,\varphi)]^2 d\varphi}, 0 \le \theta \le 2\pi$$

The rotational autocorrelation above was normalized to have a value of 1 at $\theta = 0$ or $\theta = 2\pi$. Bicubic interpolation was used for subpixel sampling when calculating the autocorrelation of pixel values from the differential image. The rotational autocorrelation of the radial FLARE component becomes:

$$G_{\text{rot,FLARE}}(r,\theta) = \frac{\int_0^{2\pi} f_{\text{FLARE}}(r)cos(2\varphi) f_{\text{FLARE}}(r)cos(2(\varphi+\theta))d\varphi}{\int_0^{2\pi}[f_{\text{FLARE}}(r)cos(2\varphi)]^2 d\varphi}$$

$$= \frac{[f_{\text{FLARE}}(r)]^2 \int_0^{2\pi} cos(2\varphi)cos(2(\varphi+\theta))d\varphi}{[f_{\text{FLARE}}(r)]^2 \int_0^{2\pi}[cos(2\varphi)]^2 d\varphi} = cos(2\theta)$$

This curve takes a local maximum at $\theta = \pi$ and local minima at $\theta = \frac{\pi}{2}$ and $\theta = \frac{3\pi}{2}$. In contrast, the autocorrelation of the noise component is expected to have a sagging profile with a minimum at $\theta = \pi$. The shape of $G_{\text{rot}}(r,\theta)$ surface calculated from actual differential images will depend on the relative intensity of the radial FLARE component

and the noise, but the presence of a peak at $\theta = \pi$ in the rotational autocorrelation will be a good indicator of the presence of the cross pattern at the radius r. The algorithms described above were packaged as an ImageJ plugin (can be found at https://gitlab.com/mkwnana/s4firp).

Obtained 2D-plots of the rotational autocorrelation for each radius were converted to 3D-plots using ImageJ's 'surface plot' function.

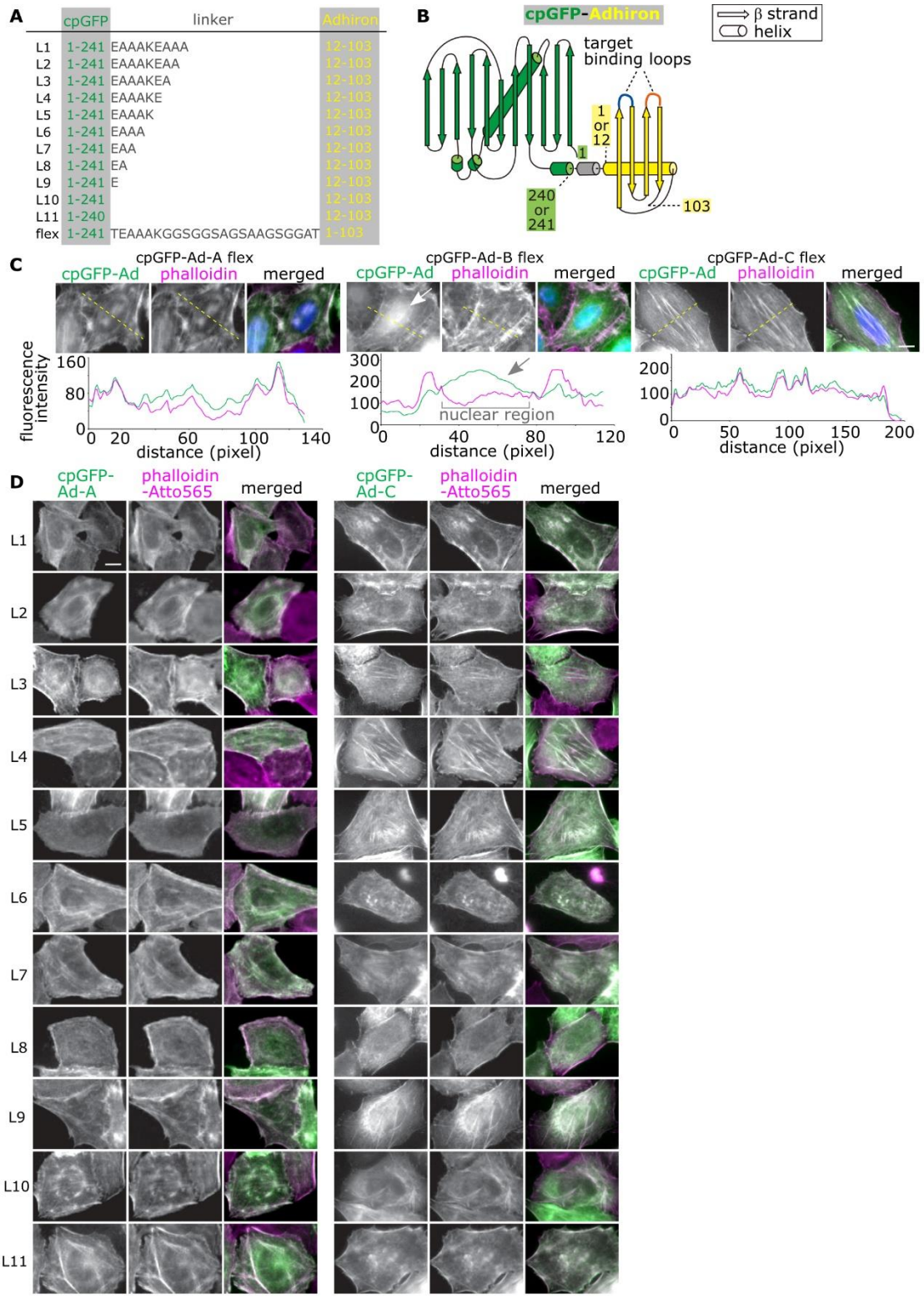
A
cpGFP
linker
Adhiron
L1 1-241 EAAAKEAAA 12-103
L2 1-241 EAAAKEAA 12-103
L3 1-241 EAAAKEA 12-103
L4 1-241 EAAAKE 12-103
L5 1-241 EAAAK 12-103
L6 1-241 EAAA 12-103
L7 1-241 EAA 12-103
L8 1-241 EA 12-103
L9 1-241 E 12-103
L10 1-241 12-103
L11 1-240 12-103
flex 1-241 TEAAAKGGSGGSAGSAAGSGGAT 1-103
B
cpGFP-Adhiron
β strand
helix
target binding loops
1 or 12
1
240 or 241
103
C
cpGFP-Ad-A flex
cpGFP-Ad-B flex
cpGFP-Ad-C flex
cpGFP-Ad
phalloidin
merged
fluorescence intensity
distance (pixel)
nuclear region
D
cpGFP-Ad-A
phalloidin-Atto565
cpGFP-Ad-C
L1
L2
L3
L4
L5
L6
L7
L8
L9
L10
L11

Fig. S1. Detailed information of cpGFP-Adhiron constructs and their localization analysis.

(A) Sequences of the linkers used in the screening are shown with the amino acid residue numbers of cpGFP and Adhiron used to create fusion proteins.

(B) Schematic representation of candidate cpGFP-Adhiron fusion proteins. Green: cpGFP, yellow: Adhiron, gray: helical linker.

(C) Top row: Representative fluorescence microscopy images of fixed HeLa cells expressing cpGFP-Ad-A/B/C flex (left panels) with phalloidin-Atto565 (middle panels) staining. Merged images of cpGFP-Adhiron (green), phalloidin-Atto565 (magenta), and DNA stained with Hoechst (blue) are also shown in the right panels. Bottom row: Intensity profiles for cpGFP-Ad-A/B/C and phalloidin-Atto565 channels along the dashed yellow lines marked on the images in top panels. Arrows show a high background in the nuclear region of cpGFP-Ad-B flex fluorescence. Scale bar: 10 μm.

(D) Co-localization analysis of cpGFP-Adhirons with actin filaments stained with phalloidin. Representative fluorescence microscopy images of fixed HeLa cells expressing cpGFP-Ad-A/C L1-L11 (left columns) with phalloidin-Atto565 (middle columns) staining are shown. Merged images of cpGFP-Adhiron (green) and phalloidin-Atto565 (magenta) are shown in the right columns. Scale bar: 10 μm.

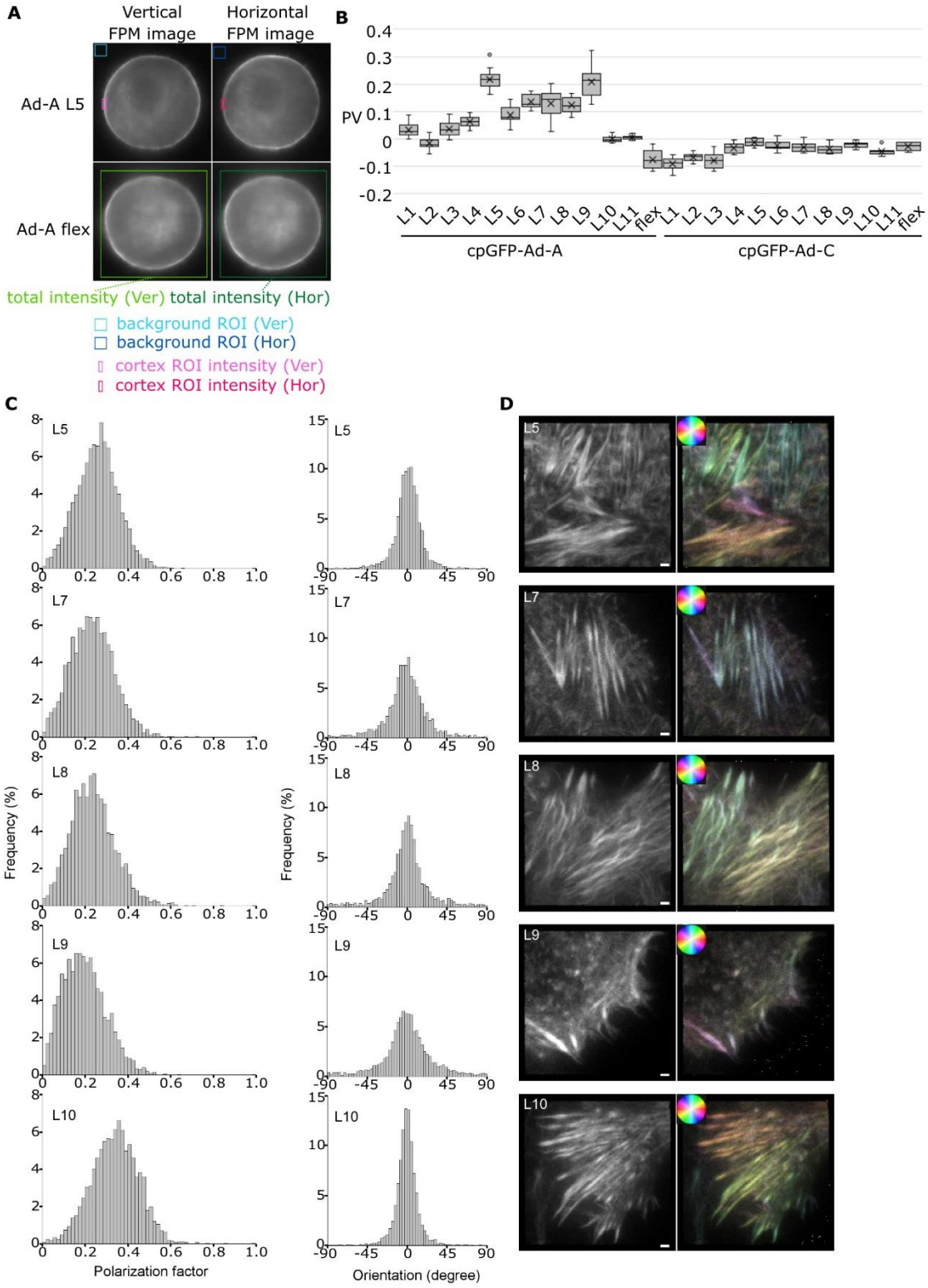
A
Vertical FPM image
Horizontal FPM image
Ad-A L5
Ad-A flex
total intensity (Ver)
total intensity (Hor)
background ROI (Ver)
background ROI (Hor)
cortex ROI intensity (Ver)
cortex ROI intensity (Hor)
B
PV
cpGFP-Ad-A
cpGFP-Ad-C
C
Frequency (%)
Polarization factor
Orientation (degree)
D

Fig. S2. Screening of cpGFP-Adhiron constructs by quantifying polarization of fluorescence in living cells.

(A) Examples of ROI settings in two-axis FPM images for calculation of Polarization Value (PV) of cpGFP-Ad-A L5 are shown. See Materials and Methods for details of PV calculation.

(B) PVs for all cpGFP-Ad constructs are shown by boxplots with cross marks indicating averages. Statistics: Student's t-test with Šidák correction. **, $P < 0.01$. n=10.

(C) Instantaneous FluoPolScope analysis of five cpGFP-Ad-A constructs (L5, 7, 8, 9, and 10) expressed in LLC-PK1 cells. Polarization factor (left) and polarization orientation (right) are shown in histograms. The ordinates of histograms are the frequencies of detected particles. Orientation at 0° indicates the polarization orientation of the particle is parallel to actin filaments, and orientation at -90° or 90° indicates the polarization orientation of the particle is perpendicular to actin filaments.

(D) Representative images of instantaneous FluoPolScope analysis. Left panels show the ensemble fluorescence intensity of four polarization orientations, and right panels show the orientation of ensemble polarization by pseudo-color. The hue color circles in the right panels show the relationship between pseudo-color and orientation of ensemble polarization. Scale bar: 1 μm.

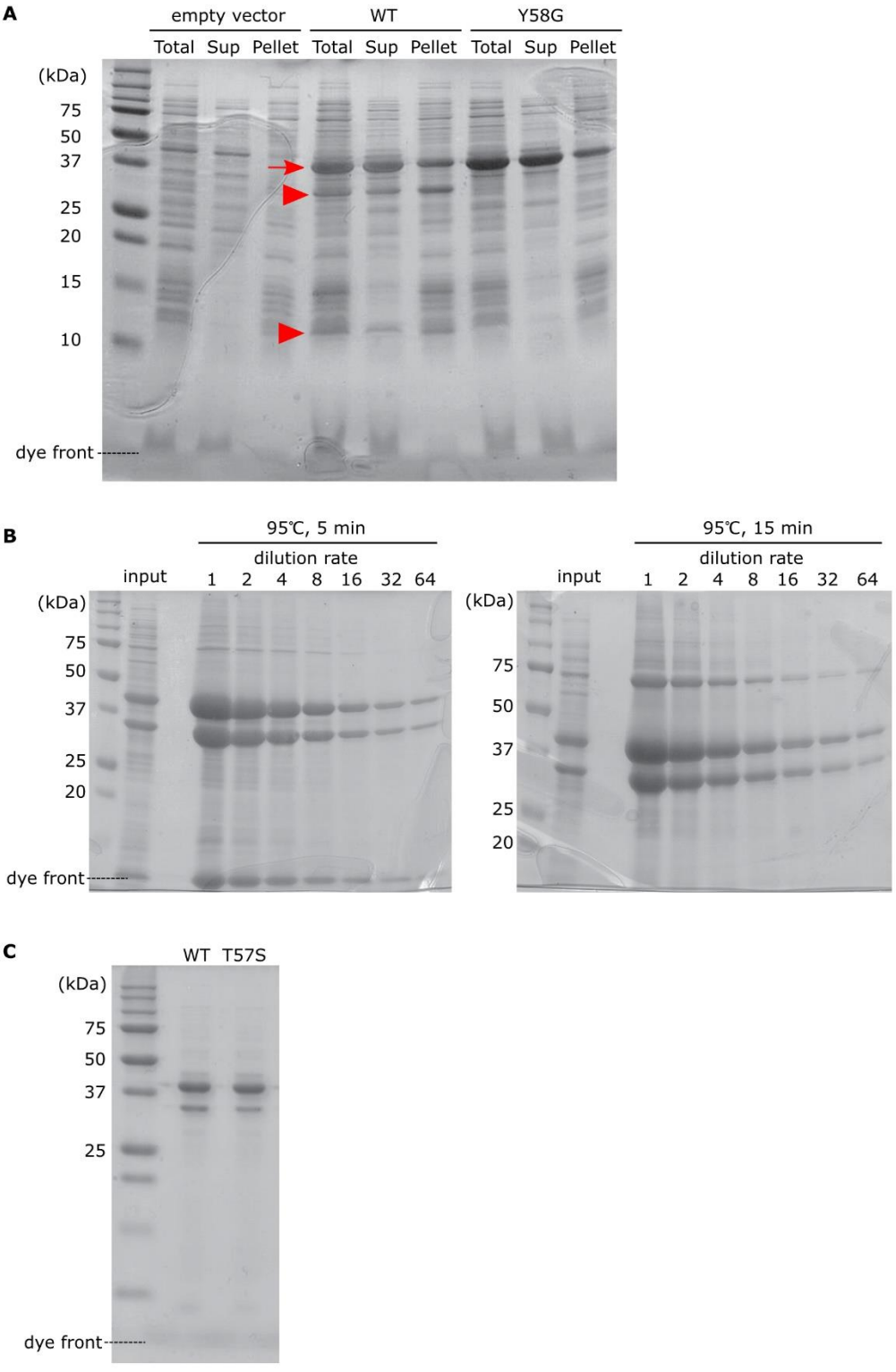
A
empty vector
WT
Y58G
Total Sup Pellet Total Sup Pellet Total Sup Pellet
(kDa)
75
50
37
25
20
15
10
dye front
B
95℃, 5 min
dilution rate
input 1 2 4 8 16 32 64
(kDa)
75
50
37
25
20
dye front
95℃, 15 min
dilution rate
input 1 2 4 8 16 32 64
(kDa)
75
50
37
25
20
C
WT T57S
(kDa)
75
50
37
25
dye front

Fig. S3. Selection of POLArIS^{act} mutants suitable for structure determination.

(A) CBB-stained SDS-PAGE gel of whole protein (Total), supernatant (Sup), and pellet of *E. coli* JM109 (DE3) bacterial cells expressing POLArIS^{act} or its Y58G variant. POLArIS^{act} protein (WT) unexpectedly produced extra bands at 32 kDa and 11 kDa (arrowheads) in addition to the expected band of 40 kDa (arrow). Extra bands disappeared when the Y58G mutant, which is expected to prevent cpGFP from forming the chromophore, was used, indicating that extra bands were produced due to "backbone fragmentation," during chromophore formation or maturation.

(B) CBB-stained SDS-PAGE gels of purified POLArIS^{act}. Proteins were purified from POLArIS^{act}-expressing bacterial cells and prepared samples were heated at 95°C for 5 min (left) or 15 min (right) and loaded onto gels with sequential dilutions. The production of extra bands shown in (A) is unlikely to be caused by the incompletion of protein denaturation, as the intensities of extra bands were not affected by the difference in the length of the heating.

(C) CBB-stained SDS-PAGE gel of purified wild-type POLArIS^{act} (WT) and its mutant (T57S) proteins. T57S mutant of POLArIS^{act} was comparatively resistant to "backbone fragmentation" and used for the crystal structure analysis.

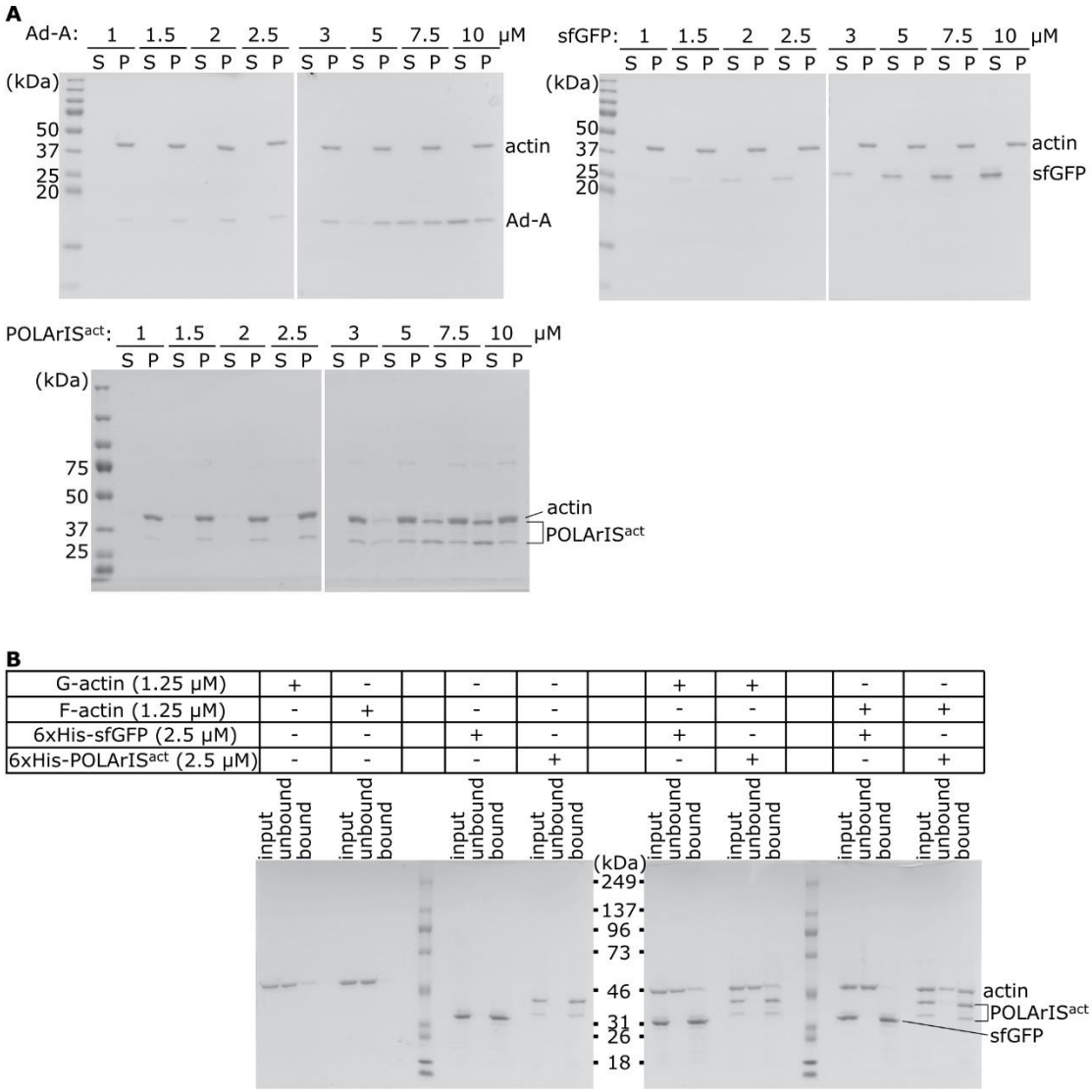

Fig. S4. Co-sedimentation and pull-down assays to analyze interaction between POLArIS^{act} and F-actin.

(A) CBB staining of typical SDS-PAGE gels of a co-sedimentation assay in which 2.5 μM F-actin were mixed with increasing concentrations of recombinant Ad-A (top left), sfGFP (top right) or POLArIS^{act} (bottom). Lanes show supernatant (S) and pellet (P) of each mixture with different concentrations of proteins.

(B) CBB staining of typical SDS-PAGE gels of actin pull-down assay. Components of each reaction are shown in the list. The bound fraction was twice as concentrated as input and unbound fractions.

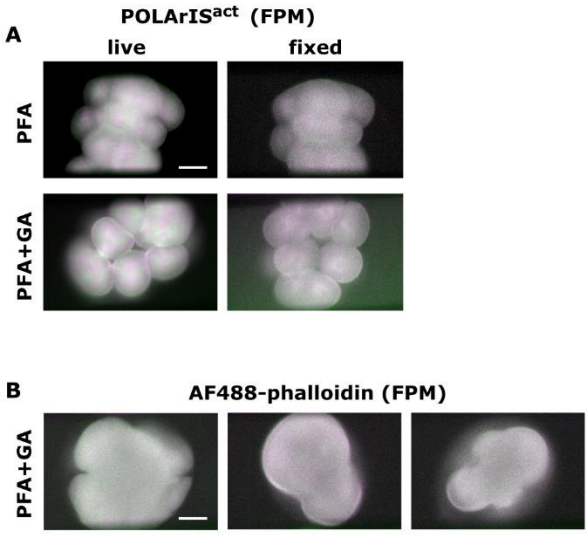

Fig. S5. Fluorescence polarization of FLARE was not preserved with PFA or PFA+GA fixatives.

(A) Green/magenta two-axis FPM images of live and fixed starfish embryos expressing POLArIS^{act} in the fourth cleavage. Soon after the green/magenta cross pattern appeared (live), the same embryos were fixed with PFA or PFA+GA (fixed) by perfusing fixative. The cross patterns of POLArIS^{act} were disappeared after fixation.

(B) Three examples of green/magenta two-axis FPM images of AF488-phalloidin staining of PFA+GA-fixed starfish embryos expressing POLArIS^{act}. The cross pattern was not visible in all embryos.

Scale bar: 50 μm.

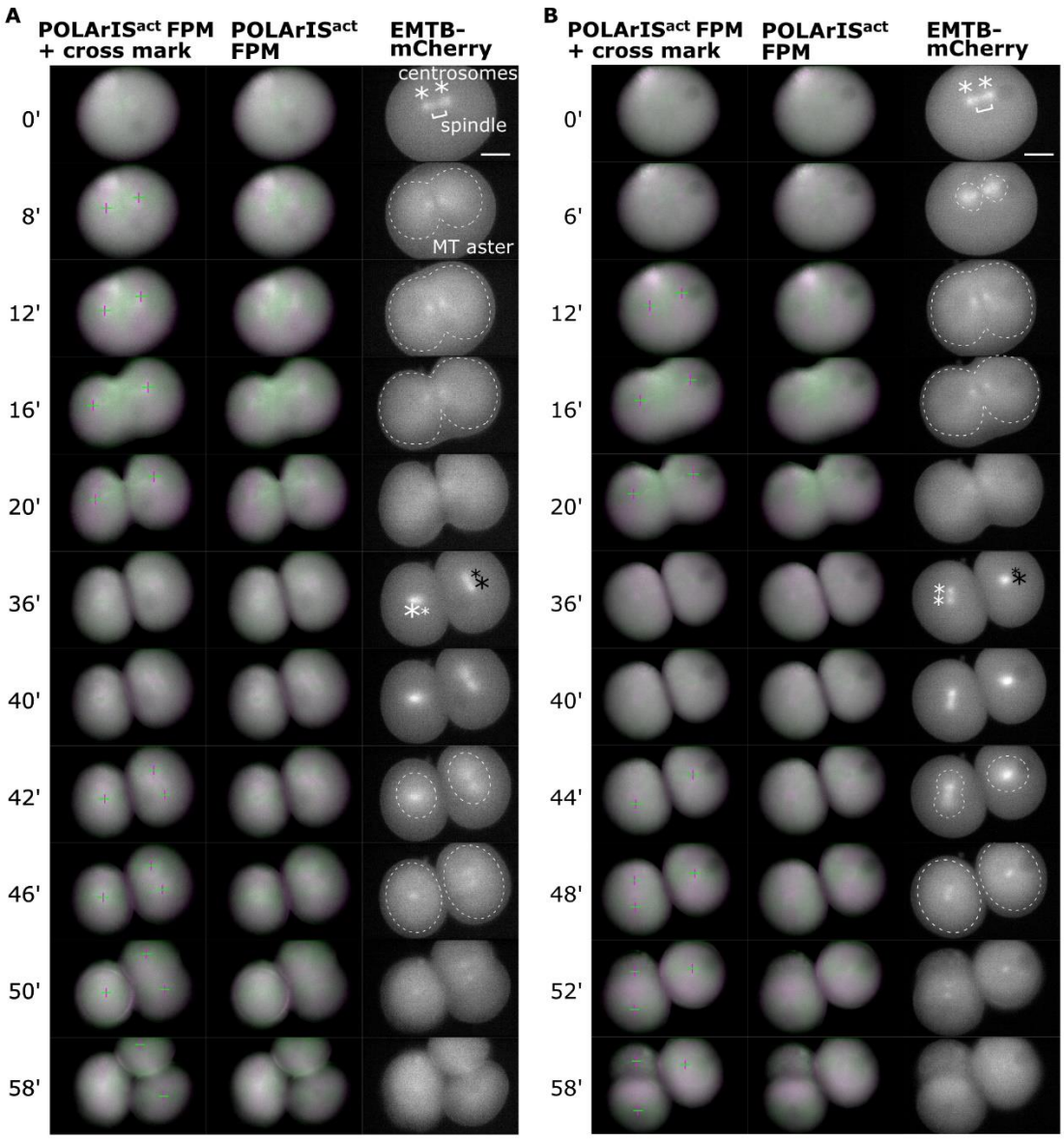

Fig. S6. Similar distribution and dynamics of FLARE and microtubule asters.

(A) Longer time-lapse green/magenta (left and middle columns) two-axis FPM images of the first and the second cleavages of the same starfish embryo expressing POLArIS^{act} and EMTB-mCherry as in Fig. 5C. The right column shows vertical polarization images of EMTB-mCherry. Cross marks (left column) indicate centers of green/magenta cross patterns. Centrosomes are shown by asterisks and contours of microtubule asters are

shown by dashed lines. In POLArIS^{act} images, the background signal was subtracted for a better presentation of cross patterns.

(B) Another example of time-lapse green/magenta (left and middle columns) two-axis FPM images of the first and the second cleavages of a starfish embryo expressing POLArIS^{act} and EMTB-mCherry.

Scale bar: 50 µm.

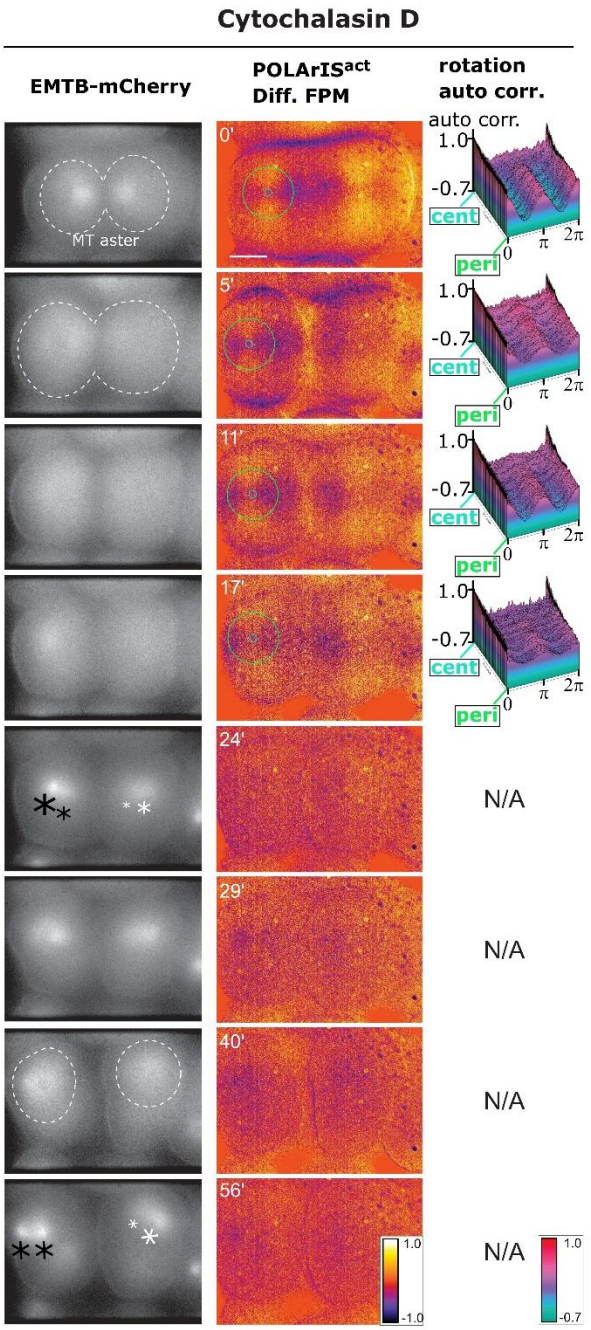

Fig. S7. Microtubule aster dynamics does not depend on FLARE.

Time-lapse two-axis FPM observation of a cytochalasin D-treated embryo expressing POLArIS^{act} and EMTB-mCherry in the fourth cleavage. The drug was added at time 0. The left column shows vertical polarization images of EMTB-mCherry, the middle column

shows differential FPM images of POLArIS^{act} with circles of min/max diameters used in autocorrelation analyses, and the right column shows 3D-plots of autocorrelation analyses of FLARE. Asterisks indicate centrosomes, dashed lines indicate contours of microtubule asters. Scale bar: 50 µm.

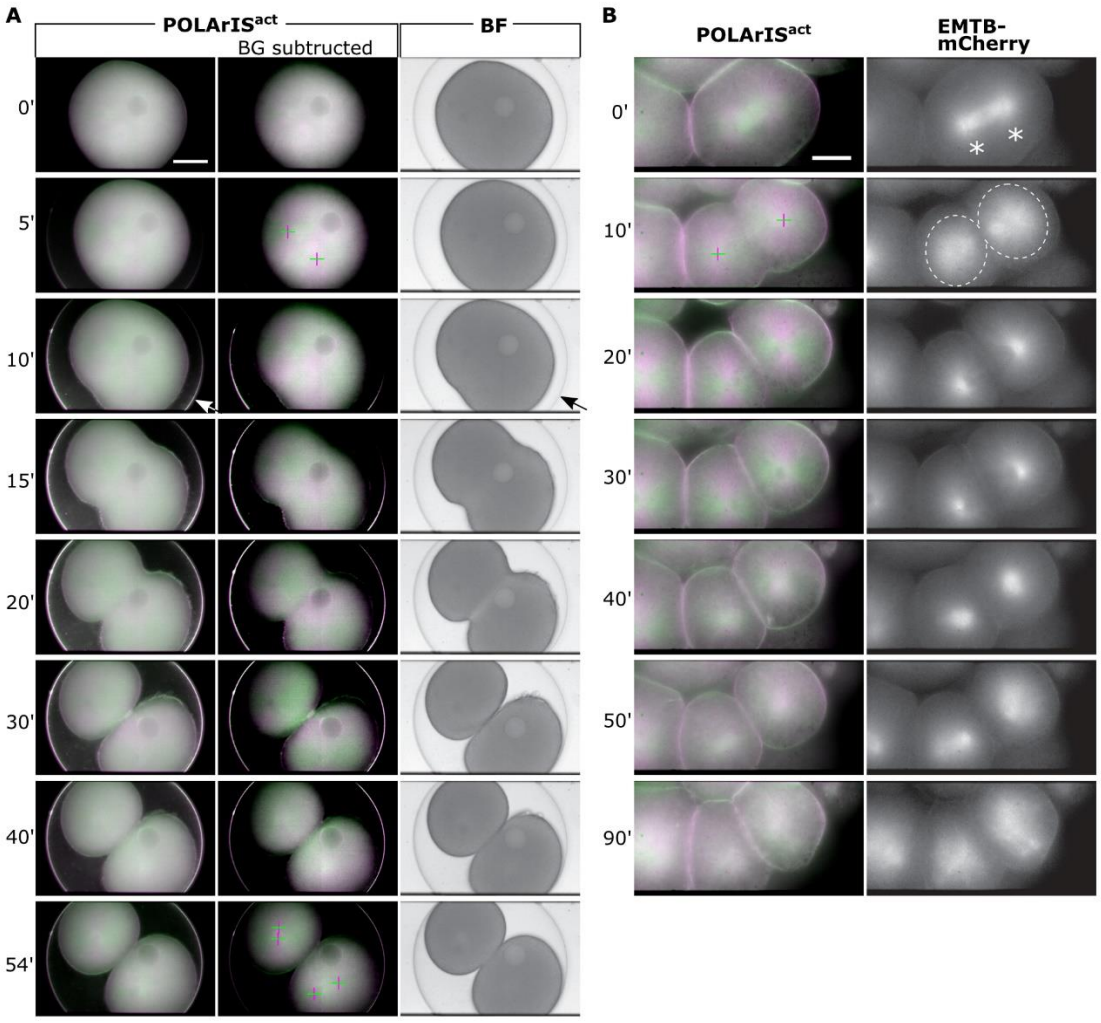

Fig. S8. Time lapse observations of SMIFH2 treated starfish embryos.

(A) A starfish embryo expressing POLArIS^{act} was treated with SMIFH2 before the first cleavage (time 0). Images by two-axis FPM (left and middle columns) and their bright-field view (right column). In panels of the middle column, the background signal was subtracted for the better presentation of green/magenta cross patterns. Arrows indicate the fertilization envelope and cross marks indicate the centers of the cross patterns of FLARE structures. Accumulation of the drug on the fertilization envelope was evident 10 min after the drug addition. Scale bar: 50 µm.

(B) A starfish embryo expressing POLArIS^{act} and EMTB-mCherry was treated with SMIFH2 and observed with two-axis FPM. SMIFH2 was microinjected and perfused under the elevated fertilization envelope. The drug was added just after microtubule asters started to extend during the fourth cleavage (time 0). The left column shows green/magenta FPM images of POLArIS^{act} and the right column shows vertical polarization images of EMTB-mCherry. Cross marks indicate the centers of the green/magenta cross patterns. Asterisks indicate centrosomes, dashed lines indicate contours of microtubule asters. Scale bar: 25 μm.

Supplementary Fig.9

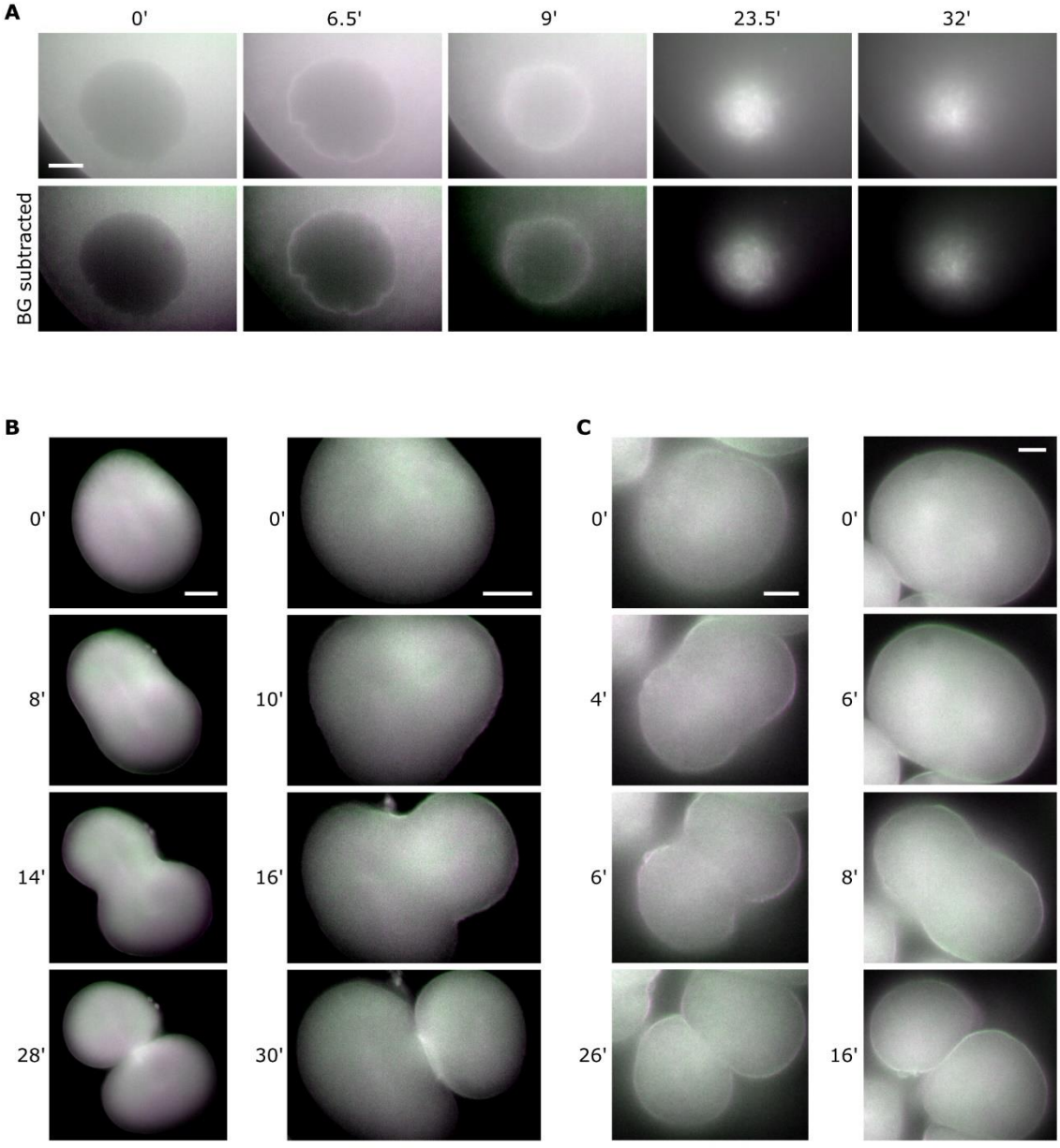

Fig. S9. Time lapse FPM observations of starfish eggs expressing UG3.

(A) Time-lapse green/magenta two-axis FPM images of starfish oocytes expressing UG3 during GV breakdown. Time 0 is just before the breakdown, approximately 30 min after

1-MA addition. In bottom panels, the background signal was subtracted for the better presentation of actin structures.

(B, C) Time-lapse green/magenta two-axis FPM images of embryo expressing UG3 in the second (B) or the fourth cleavages (C).

Scale bars: 25 μm (A, C), 50 μm (B).

Table S1. Data Collection and Refinement Statistics.

Data collection and processing	
Beamline	X06DA, SLS
Space group	$I\ 2_1\ 2_1\ 2_1$
Unit-cell parameter	
a, b, c (Å)	78.1, 113.6, 132.7
α, β, γ (˚)	90.0, 90.0, 90.0
Wavelength (Å)	1.000
Resolution range (Å)	50.0–2.50 (2.64–2.50)
Redundancy	7.1 (7.1)
Completeness (%) [a]	99.9 (99.8)
R_{sym} [b] (%) [a]	1.62 (9.6)
I/σ (I) [a]	13.3 (1.0)
No. monomers/asymmetric unit	1
Model refinement	
No. of reflections	20785
No. of protein atoms	2528
No. of water molecules	81
R_{work}/R_{free} (%)	21.4/23.8
r.m.s.d. for bond length (Å)	0.003
r.m.s.d. for bond angles (˚)	0.633
Residues in the Ramachandran plot	
Favored region (%)	95.7
Allowed regions (%)	2.6
PDB ID	7C03

[a] Statistics for the highest resolution shell are given in parentheses.

[b] $R_{sym} = \sum_{hkl} \sum_i |I_i(hkl) - \langle I(hkl) \rangle| / \sum_{hkl} \sum_i I_i(hkl)$.

Movie S1 (separate file).

A representative movie of the single-particle observation of POLArIS^{act} with Instantaneous FluoPolScope in a lamellipodium of a living XTC cell expressing POLArIS^{act}. Left panels show the ensemble fluorescence intensity of instantaneous FluoPolScope and right panels show the polarization factor and the orientations of polarized fluorescence (indicated by yellow lines, yellow scale bar shows the maximum polarization factor) of detected POLArIS^{act} particles (yellow circles). x312 actual speed.

Movie S2 (separate file).

Time-lapse of two-axis FPM (green/magenta) of starfish oocytes expressing POLArIS^{act} during the breakdown of the GV and formation of the F-actin meshwork, related to Fig. 3A. Time 0 is just before the breakdown, about 27 min after 1-MA addition. Arrow indicates GV, and arrowheads indicate actin filaments with clear polarization in the meshwork (green: horizontal, magenta: vertical). x236 actual speed.

Movie S3 (separate file).

Time-lapse of starfish oocytes expressing POLArIS^{act} during the polar body extrusion with two-axis green/magenta FPM (left) and bright-field view (right), related to Fig. 3B. The positions of the polar body extrusion and the accumulation of contractile ring-like F-actin are shown by arrowhead and arrow, respectively. x312 actual speed.

Movie S4 (separate file).

Fluorescence microscopy time-lapse of the fertilization of starfish oocyte expressing POLArIS^{act} with Hoechst staining, related to Fig. 3D. Top shows the entire egg, and bottom magnifies the area where the actin bundle, DNA of the egg (arrowheads) and sperm (arrows) were observed. Left: POLArIS^{act}, middle: Hoechst, right: merged (POLArIS^{act}: green, Hoechst: magenta). x240 actual speed.

Movie S5 (separate file).

Time-lapse during the first cleavage of a starfish embryo expressing POLArIS^{act} with two-axis FPM (green/magenta), related to Fig. 4A. In the first half, cross marks indicate the centers of the green/magenta cross patterns. These illustrations are omitted from the second half. x505 actual speed.

Movie S6 (separate file).

Time-lapse during the first cleavage of a starfish embryo expressing POLArIS^{act} with differential FPM shown in grayscale, created from the same data of Movie S5 for better visualization of FLARE.

Movie S7 (separate file).

Overnight time-lapse two-axis FPM (green/magenta) after the fourth cleavage of a starfish embryo expressing POLArIS^{act}, related to Fig. 4B. Cross marks indicate the centers of the green/magenta cross patterns. x612 actual speed.

Movie S8 (separate file).

Overnight time-lapse differential FPM after the fourth cleavage of a starfish embryo expressing POLArIS^{act}, created from the same data of Movie S7 for better visualization of FLARE.

Movie S9 (separate file).

Time-lapse green/magenta FPM movie of the first cleavage of a starfish embryo expressing POLArIS^{act} and EMTB-mCherry, related to Fig. 5C. For EMTB-mCherry, only vertical polarization images were shown. In the first half, cross marks indicate the centers of FLARE, and asterisks and dashed lines indicate centrosomes and contours of microtubule asters, respectively. These illustrations are omitted from the second half. x900 actual speed.

Movie S10 (separate file).

Time-lapse differential FPM movie of the first cleavage of a starfish embryo expressing POLArIS^{act} and EMTB-mCherry, created from the same data of Movie S9 for better visualization of FLARE. Only POLArIS^{act} images were shown.

Movie S11 (separate file).

Time-lapse green/magenta FPM movie of the third cleavage of a starfish embryo expressing POLArIS^{act} and EMTB-mCherry, related to Fig. 6B. For EMTB-mCherry, only vertical polarization images were shown. Nocodazole was added at time 0. x150 actual speed.

SI References

1. A. Lopata, *et al.*, Artificial actin-binding proteins with novel multifunctional properties. *Biophisical Soc. 60th Annu. Meet.*, L3598-Pos, Los Angeles, California, 02 Mar (2016).
2. N. Nakai, *et al.*, Genetically encoded orientation probes for F-actin for fluorescence polarization microscopy. *Microscopy* **68**, 359–68 (2019).
3. Y. Zhao, *et al.*, An expanded palette of genetically encoded Ca^{2+} indicators. *Science* **333**, 1888–91 (2011).
4. W. Kabsch, XDS. *Acta Crystallogr. Sect. D* **66**, 125–32 (2010).
5. A. J. McCoy, *et al.*, Phaser crystallographic software. *J. Appl. Crystallogr.* **40**, 658–74 (2007).

6. P. D. Adams, *et al.*, PHENIX: A comprehensive Python-based system for macromolecular structure solution. *Acta Crystallogr. Sect. D Biol. Crystallogr.* **66**, 213–21 (2010).

7. P. Emsley, B. Lohkamp, W. G. Scott, K. Cowtan, Features and development of Coot. *Acta Crystallogr. Sect. D Biol. Crystallogr.* **66**, 486–501 (2010).

8. M. D. Winn, *et al.*, Overview of the CCP4 suite and current developments. *Acta Crystallogr. Sect. D Biol. Crystallogr.* **67**, 235–42 (2011).

9. E. F. Pettersen, *et al.*, UCSF Chimera - A visualization system for exploratory research and analysis. *J. Comput. Chem.* **25**, 1605–12 (2004).

10. K. N. Richter, *et al.*, Glyoxal as an alternative fixative to formaldehyde in immunostaining and super-resolution microscopy. *EMBO J.* **37**, 139–59 (2018).

11. S. B. Mehta, *et al.*, Dissection of molecular assembly dynamics by tracking orientation and position of single molecules in live cells. *Proc. Natl. Acad. Sci.* **113**, E6352–E6361 (2016).